

Rényi Entropies from Random Quenches in Atomic Hubbard and Spin Models

A. Elben,^{1, 2, *} B. Vermersch,^{1, 2, *} M. Dalmonte,³ J. I. Cirac,⁴ and P. Zoller^{1, 2, 4}

¹*Institute for Theoretical Physics, University of Innsbruck, Innsbruck, Austria*

²*Institute for Quantum Optics and Quantum Information,
Austrian Academy of Sciences, Innsbruck, Austria*

³*International Center for Theoretical Physics, 34151 Trieste, Italy*

⁴*Max-Planck-Institut für Quantenoptik, Hans-Kopfermann-Str. 1, D-85748 Garching, Germany*

(Dated: April 25, 2022)

We present a scheme for measuring Rényi entropies in generic atomic Hubbard and spin models using single copies of a quantum state and for partitions in arbitrary spatial dimension. Our approach is based on the generation of random unitaries from random quenches, implemented using engineered time-dependent disorder potentials, and standard projective measurements, as realized by quantum gas microscopes. By analyzing the properties of the generated unitaries and the role of statistical errors, with respect to the size of the partition, we show that the protocol can be realized in existing AMO quantum simulators, and used to measure for instance area law scaling of entanglement in two-dimensional spin models or the entanglement growth in many-body localized systems.

Atomic physics provides us with the realization of engineered quantum many-body lattice models. This includes Hubbard models for bosonic and fermionic cold atoms in optical lattices [1], and spin models with Rydberg atoms [2] and chains of trapped ions [3]. Among the noticeable recent experimental advances are quantum control, and single shot measurements in lattice systems of atoms [4–11] and ions [12, 13] achieving *single site resolution*, as illustrated for atoms in optical lattices by the quantum gas microscope [14]. This provides us not only with a unique atomic toolbox to prepare equilibrium and non-equilibrium states of quantum matter, but also with the opportunity to access in experiments novel classes of observables, beyond the familiar low order correlation functions. An outstanding example is the measurement of Rényi entropies, defined as $S^{(n)}(\rho_A) = \frac{1}{1-n} \log \text{Tr}(\rho_A^n)$ ($n > 1$) with ρ_A the reduced density matrix of a subsystem $A \subset \mathcal{S}$ of a many-body system \mathcal{S} , which gives us a unique signature of entanglement properties in many-body phases and dynamics [15], and is also of interest in the ongoing discussion on ‘quantum supremacy’ [16–20].

Below we will describe a protocol for measuring Rényi entropies based on *random measurements* [21]. In our approach the required *random unitaries* are realized using the same AMO toolbox which underlies the preparation of quantum phases and dynamics (c.f. Fig. 1). This enables a physical implementation of the protocol, applicable to generic Hubbard and spin models and in arbitrary dimension. We emphasize that in contrast to recent protocols to measure n -th order Rényi entropies, which requires preparation of n identical copies of the quantum system [22–25], a random measurement protocol requires only a single quantum system [21], and thus can be implemented directly with existing AMO experimental setups, and extended to solid state platforms [26, 27]. A central aspect in any measurement scheme for Rényi entropies,

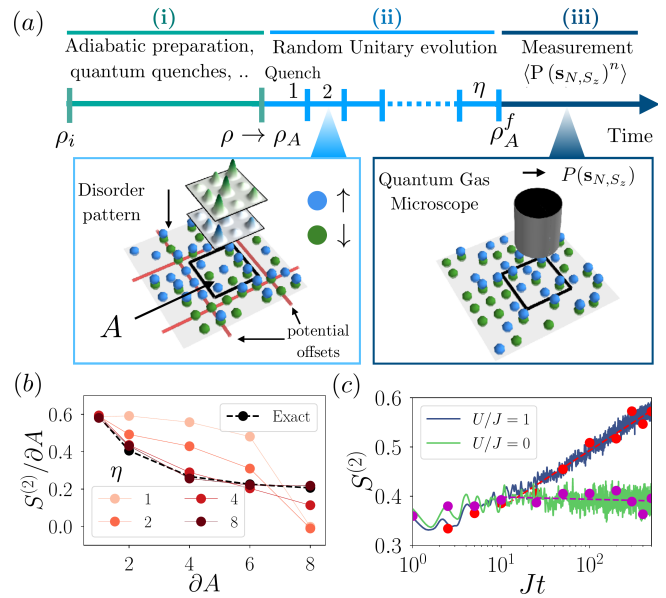


FIG. 1. *Protocol for measuring Rényi entropies via random quenches.* (a) Experimental sequence consisting of a preparation of quantum state ρ (i), random unitary evolution via random quenches on the partition A (ii), and measurements in a fixed basis (iii). (b) Application to the measurement of $S^{(2)}(\rho_A)$ for the ground state of the 2D Heisenberg model with 8×8 sites. The estimated entropy shows the area law scaling at large depth η . (∂A is the A perimeter). The quench parameters are $\delta = J = 1/T$. (c) Entanglement growth in the MBL phase of the unidimensional BH model, averaged over 250 disorder realizations, quench time $JT = 1$ and $\eta = 20$. Shown is the logarithmic growth of $S^{(2)}(\rho_A)$ at half partition with time in a system with 10 sites and 5 particles. The exact value of $S^{(2)}(\rho_A)$ (solid lines) is compared to the estimated values (dots). The dashed lines are linear fits to the estimated values. For (b-c), we consider $N_U = N_M = 100$.

* These two authors contributed equally.

as for a full quantum state tomography [28–30], is scaling of the experimental effort with size of the system of interest: below we provide a detailed analysis and feasi-

bility study of required resources in terms of number of measurements and random unitaries, and verification of random unitaries.

Random measurements to infer Rényi entropies have been discussed in a quantum information context [21]. For qubits, the protocol consists in applying to ρ_A a *random unitary* matrix U_A from the circular unitary ensemble (CUE), which can be implemented on a quantum computer as a random sequence of two-qubit gates [31, 32]. The measurement of the probabilities $P(\mathbf{s}) = (\rho_A^f)_{\mathbf{ss}}$, with $\rho_A^f = U_A \rho_A U_A^\dagger$ and \mathbf{s} the qubit states in the computational basis, then allows us to infer Rényi entropies $S^{(n)}(\rho_A)$ from the statistical moments $\langle P(\mathbf{s})^n \rangle$, with $\langle \dots \rangle$ the ensemble average over the random unitaries. In particular, for $n = 2$ we have $S^{(2)}(\rho_A) = -\log [\mathcal{N}_A(\mathcal{N}_A + 1)\langle P(\mathbf{s})^2 \rangle - 1]$ with \mathcal{N}_A the Hilbert space dimension of A [33]. This relies on the identity for unitary 2-designs [34, 35]

$$\langle u_{\mathbf{s}\mathbf{i}_1} u_{\mathbf{s}\mathbf{i}_2}^* u_{\mathbf{s}\mathbf{i}_3} u_{\mathbf{s}\mathbf{i}_4}^* \rangle = \frac{\delta_{\mathbf{i}_1, \mathbf{i}_2} \delta_{\mathbf{i}_3, \mathbf{i}_4} + \delta_{\mathbf{i}_1, \mathbf{i}_4} \delta_{\mathbf{i}_2, \mathbf{i}_3}}{\mathcal{N}_A(\mathcal{N}_A + 1)}, \quad (1)$$

with $(u)_{\mathbf{ij}}$ the matrix elements of U_A . In a similar way, higher order Rényi entropies are obtained from n -th order correlators of the CUE (discussed as n -designs) [35].

We realize random unitaries as a *series of quenches* in interacting Hubbard and spin models with *engineered disorder* for the subsystem A ,

$$U_A = e^{-iH_A^\eta T} \cdots e^{-iH_A^1 T}, \quad (2)$$

to be followed by a readout with a quantum gas microscope (see Fig. 1). Here H_A^j denotes the Hamiltonian for a given disorder pattern j , and we consider η quenches, each of duration T , and $T_{\text{tot}} \equiv \eta T$ the total interaction time. The questions to be addressed are then: (i) the convergence to the CUE in terms of n -designs (c.f. Eq. (1)), in view of the experimentally available disorder Hamiltonians, and ‘depth’ η , and experimental verification; and (ii) the scaling of statistical errors with the number of measurements N_M and unitaries N_U . We emphasize the relation of (i) to the ongoing theoretical [36–40] and experimental [41] discussion of thermalization dynamics of periodically driven quantum many-body systems, and their connection to quantum chaos [42]. The type of problems, which can be addressed with our protocol are illustrated in Fig. 1(b,c), where we present results simulating the *measurement of an area law* for a 2D-Heisenberg model [43], and ‘seeing’ entropy growth in many-body localized [44–46] (MBL) dynamics in the Bose-Hubbard (BH) model (for details see below).

Protocol for the Fermi-Hubbard model. – In view of recent progress in realizing the 2D Fermi Hubbard (FH) model [5–8], and in building a Fermi gas microscope we wish to illustrate the protocol for spinful fermions in a 2D optical lattices (c.f. Fig. 1(a)). We show below how to adapt the method to Bose-Hubbard and Quantum Ising models (for example). The FH Hamiltonian as a sum of

hopping and interaction terms is

$$H_F = -t_F \sum_{\langle \mathbf{i}, \mathbf{l} \rangle \in \mathcal{S}, \sigma} c_{\mathbf{i}\sigma}^\dagger c_{\mathbf{l}\sigma} + U \sum_{\mathbf{i} \in \mathcal{S}} n_{\mathbf{i}\uparrow} n_{\mathbf{i}\downarrow}. \quad (3)$$

with hopping amplitude t_F , and interaction strength U . Here $c_{\mathbf{i}, \sigma}^{(\dagger)}$ denote fermionic annihilation (creation) operators at lattice site $\mathbf{i} = (i_x, i_y)$ and spin $\sigma \in \{\uparrow, \downarrow\}$, and $n_{\mathbf{i}\sigma} = c_{\mathbf{i}\sigma}^\dagger c_{\mathbf{i}\sigma}$. We will add disorder below to realize H_A^j .

The measurement sequence is shown in Fig. 1(a): (i) A (non-)equilibrium quantum many body state ρ of interest is prepared for the the full system \mathcal{S} based on Eq. (3). (ii) Isolation of the partition A of dimension (L_x, L_y) , with $L \equiv L_x L_y$ the number of isolated sites, is obtained via spatial addressing (c.f. Fig. 1(a)). The Hamiltonian H_j is realized as restriction $H_A^j = H_F|_A + \sum_{\mathbf{i} \in A, \sigma} \Delta_{\mathbf{i}, \sigma}^j n_{\mathbf{i}\sigma}$ and with random lattice offsets $\Delta_{\mathbf{i}, \sigma}^j$. In view of particle and spin conservation in H_F , U_A , as given by Eq. (2), decomposes into blocks with different total particle number N and magnetization S_z , $U_A = \bigoplus_{N, S_z} U_A^{(N, S_z)}$ and $\rho_A = \bigoplus_{N, S_z} \rho_A^{(N, S_z)}$. Below we study in each block the realization of a random unitary $U_A^{(N, S_z)}$ corresponding to an n -design ($n = 2, 3, \dots$) as function of η and T_{tot} . (iii) The probabilities $P(\mathbf{s}_{N, S_z})$ as lattice site occupations are measured with a quantum gas microscope, where the states $\mathbf{s}_{N, S_z} = (n_{\mathbf{i}, \uparrow}, n_{\mathbf{i}, \downarrow})_{\mathbf{i}}$ satisfy $N = \sum_{\mathbf{i} \in A} (n_{\mathbf{i}\uparrow} + n_{\mathbf{i}\downarrow})$ and $S_z = \sum_{\mathbf{i} \in A} (n_{\mathbf{i}\uparrow} - n_{\mathbf{i}\downarrow})$. These probabilities can be estimated via a sequence of N_M projective measurements [47]. We note that, as shown in the supplementary material [48] (SM), our protocol can also be realized using other observables. By repeating this procedure for different random unitaries, we can finally estimate the ensemble averages $\langle P(\mathbf{s}_{N, S_z})^n \rangle$, which are related to functionals of the density matrix ρ_A [21]. Using respectively 1- and 2-design properties, one finds

$$\langle P(\mathbf{s}_{N, S_z}) \rangle = \frac{\text{Tr} [\rho_A^{(N, S_z)}]}{\mathcal{N}_A^{(N, S_z)}}, \quad (4)$$

$$\langle P(\mathbf{s}_{N, S_z})^2 \rangle = \frac{\text{Tr} [\rho_A^{(N, S_z)}]^2 + \text{Tr} [\rho_A^{(N, S_z)2}]}{\mathcal{N}_A^{(N, S_z)} (\mathcal{N}_A^{(N, S_z)} + 1)}, \quad (5)$$

where $\mathcal{N}_A^{(N, S_z)}$ is the Hilbert space dimension of the particle-spin block in the subsystem A . Hence, from estimations of $\langle P(\mathbf{s}_{N, S_z})^n \rangle$, ($n = 1, 2$), $\text{Tr} [\rho_A^{(N, S_z)2}]$ can be extracted. By summation over all particle-spin sectors, one obtains the total purity $p_2 \equiv \text{Tr} [\rho_A^2] = \sum_{N, S_z} \text{Tr} [\rho_A^{(N, S_z)2}]$ and finally the second Rényi entropy $S^{(2)}(\rho_A)$. Higher order ensemble averages $\langle P(\mathbf{s}_{N, S_z})^n \rangle$ are related to higher order powers $p_n \equiv \text{Tr} (\rho_A^{(N, S_z)n})$ and Rényi entropies. In the following, we focus on generation of unitaries and statistical errors for second order Rényi entropies $S^{(2)}(\rho_A)$, and refer to the SM [48] for the general case.

Generation of random unitaries. – Below we present a numerical study of generation of approximate unitary 2-designs [53, 59, 60], focusing on convergence of the U_A [c.f. Eq. (2)] to the CUE as function of time $T_{\text{tot}} = \eta T$, and of the depth η of the ‘random circuit’. While the full system \mathcal{S} can be arbitrary large, we emphasize that — in view of the scaling of statistical errors with the partition size A (see below) — the applicability of the protocol in an actual experiment will *a priori* be limited to domains A of moderate size, which are within range of accurate numerical simulations. For this reason, we will consider test states ρ_A in A to carry out our numerical analysis and in particular to extract the scaling of errors. We then discuss the physical examples presented in Fig. 1(b-c), where ρ_A is extracted from a many-body quantum state $\rho = |\psi\rangle\langle\psi|$ of interest. Below we present results for the Heisenberg model in 1D and 2D, which allows larger partition sizes, and we refer to Ref. [48] for the FH model. The Hamiltonian is $H_h = J \sum_{\langle\mathbf{i}\mathbf{l}\rangle} \sigma_{\mathbf{i}} \cdot \sigma_{\mathbf{l}}$, with nearest neighbor interactions, as obtained from Eq. (3) in the limit of strong interactions $U \gg t_F$ at half filling (or alternatively with Rydberg atoms [61] or trapped ions [62]). Here, $\sigma_{\mathbf{i}}$ are the Pauli matrices at lattice site \mathbf{i} , and $J = t_F^2/U$ is the superexchange interaction. To realize the random unitaries via Eq. (2), we consider disorder potentials $\delta_{\mathbf{i}}^j = \Delta_{\mathbf{i}\uparrow}^j - \Delta_{\mathbf{i}\downarrow}^j$ drawn for each quench j from a normal distribution with standard deviation δ , i.e. $H_A^j \equiv H_h|_A + \sum_{\mathbf{i} \in A} \delta_{\mathbf{i}}^j \sigma_{\mathbf{i}}^z$ [63].

Fig. 2(a-f) shows the error of the estimated purity $(p_2)_e$ of various test states ρ_A (defined in the caption) for partitions A of various sizes L in 1D ($L = L_x$) and 2D ($L = L_x L_y$) [64]. According to panels (a,b,c), for a fixed quench time $JT = 1$ and disorder strength $\delta = J$, the error decreases exponentially with growing $JT_{\text{tot}}/L = \eta/L$ towards a plateau, which corresponds to the statistical error threshold (see below). Thus our results indicate ‘efficient’ convergence of U_A to an approximate 2-design, after a total time T_{tot} which scales linearly with system size, as in conventional random circuits based on engineered gates [53, 59, 60]. Note that our simulations show that product states, which can easily be prepared in an experiment with high fidelity, provide good indicators of convergence of the generated unitaries.

For a given total time T_{tot} , which in an experiment is set by the finite coherence time, we show in panel Fig. 2(d) the existence of optimal quench parameters $JT \approx 1$ to minimize errors in the estimated purity. This reflects the trade-off between the requirements of (i) to evolve the system for each quench j during a time sufficiently large compared to timescales J^{-1}, δ^{-1} set by the Hamiltonian [65], i.e. to prevent a quantum Zeno effect, and (ii) to change the disorder pattern frequently to prevent many-body localization. It also exists an optimal disorder strength $\delta \approx J$ [48], resulting from a tradeoff between localizing effects in the limit $\delta \gg J$ and a vanishing random component of the applied quenches in the limit $\delta \ll J$. We note that the use of a single disorder pattern, combined with random quench times $T \rightarrow T_j$,

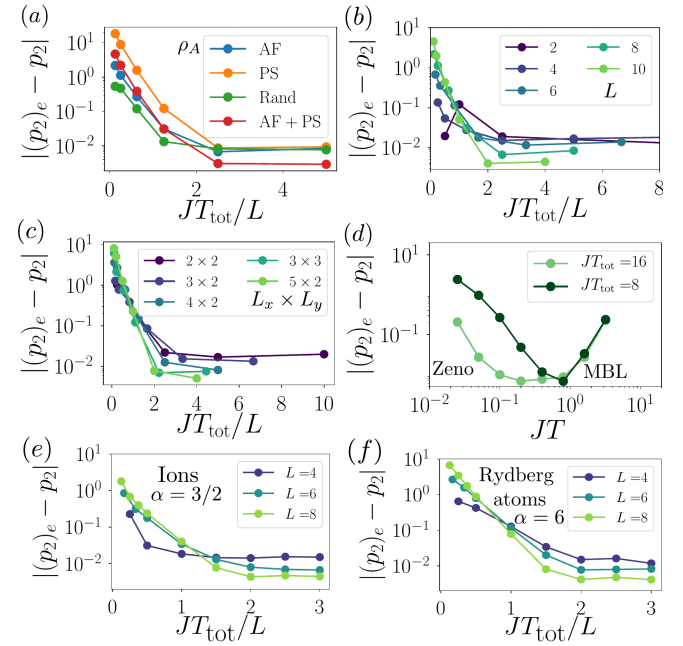


FIG. 2. *Creation of approximate 2-designs in Heisenberg (a-d) and Quantum Ising models (e-f).* (a) Average error of the estimated purity $|(p_2)_e - (p_2)|$ for a uni-dimensional partition of size $L = 8$ and various test states: an antiferromagnetic state $|\psi_{\text{AF}}\rangle$, the phase separated state $|\psi_{\text{PS}}\rangle = \prod_{\mathbf{i}, i_x \leq L_x/2} |\downarrow\rangle_{\mathbf{i}} \prod_{\mathbf{i}, i_x > L_x/2} |\uparrow\rangle_{\mathbf{i}}$, a pure random state $|\psi_{\text{rand}}\rangle$ with $S_z = 0$, and the mixed state $\rho_A = \frac{1}{2}(|\psi_{\text{AF}}\rangle\langle\psi_{\text{AF}}| + |\psi_{\text{PS}}\rangle\langle\psi_{\text{PS}}|)$. (b-c) Error for $\rho_A = |\psi_{\text{AF}}\rangle\langle\psi_{\text{AF}}|$ for (b) uni-dimensional partitions ($L = L_x$) and (c) two-dimensional partitions ($L = L_x L_y$). (d) Optimization of the quench time JT for fixed total time T_{tot} and disorder strength $\delta = J$. (e-f) Error of the estimated purity of $|\Psi_{\text{AF}}\rangle$ in the long range Quantum Ising model with power law exponents $\alpha = 1.5$ (e) and $\alpha = 6$ (f), as realized with trapped ions and Rydberg atoms, respectively. For all panels, we average over $N_U = 500$ unitaries and consider $N_M = \infty$.

represents a complementary possibility to generate the required random unitaries [48].

Our findings, in particular the convergence to approximate 2-designs and the corresponding scalings, also apply to generic Fermi and Bose Hubbard models, and quantum Ising models [48]. We illustrate this in Fig. 2 (e-f) for the long-range quantum Ising model in 1D, as realized with trapped ions [12, 13] [interaction power law exponent $\alpha = 1.5$ (e)] and Rydberg atoms [9–11] [(f) $\alpha = 6$]. Note that interactions of longer range increase the rate of convergence to 2-designs due to a higher connectivity. Moreover, we emphasize that (i) our measurement scheme does not rely on the knowledge of the applied unitaries U_A , i.e. of the knowledge of the disorder patterns δ_j^i , and (ii) — with respect to state-of-the-art atomic Hubbard and spin experimental setups — the measurement protocol is robust against the imperfect reproducibility of the generated unitaries and decoherence [48]. While we are interested in this work in the limit of large times

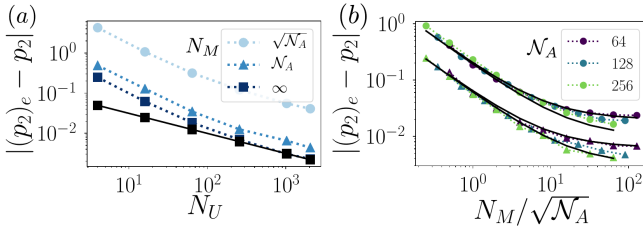


FIG. 3. *Scaling of statistical errors.* (a) Average statistical error of the estimated purity as a function of N_U for various N_M , $N_A = 256$. (b) Error as a function of N_M , for different N_A , showing birthday paradox scaling $N_M/\sqrt{N_A}$. Circles represent $N_U = 100$ and triangles $N_U = 1000$. The unitaries are sampled from the CUE numerically [57]. The black lines represent the expressions given in Ref. [48].

T_{tot} where approximate 2-designs are created (as part of our measurement scheme), we finally remark that random quenches in AMO systems also provide an experimental platform to study fast thermalization dynamics towards quantum chaos [48], but also to characterize the entanglement growth, associated with random time evolution [66].

Statistical errors – We now discuss the statistical errors due to a finite number of random unitaries N_U and of measurements N_M per unitary.

For simplicity, we assume in the following that $\rho_A = \rho_A^{(N, S_z)}$ describes a state in a single spin-particle sector with dimension $N_A^{(N, S_z)}$, where random unitaries from exact 2-designs are created. Since the following discussion is not specific to an underlying physical model, we also drop the labels (N, S_z) . With respect to measurement of purities, we find that the average statistical error scales, for $N_U \gg 1$, as $|(p_2)_e - p_2| \sim (C_2 + N_A/N_M)/\sqrt{N_A N_U}$ [48], where $C_2 = \mathcal{O}(1)$ is largest for pure states. The first term, which is independent of N_M , arises from the average over a finite number N_U of random unitaries [21]. The second originates from the finite number N_M of measurements per random unitary. It leads to a requirement of $N_M \sim \sqrt{N_A}$ to determine the purity up to an error of the order $1/\sqrt{N_U}$ [67]. This type of scaling is directly related to the average number of doublons obtained when sampling a discrete variable (the birthday paradox [68]). The analytical findings are confirmed by the numerical experiments presented in Fig. 3. In panel (a), the average error of the purity is shown as a function of N_U , decreasing as $1/\sqrt{N_U}$ for fixed N_M . In panel (b), it is represented as a function of N_M , for $N_U = 100$ and 1000.

The total number of measurements N_M scales polynomially with the Hilbert space dimension N_A , and thus exponentially with the size of A (without constraints on the size of the total system S). However, compared to e.g. full quantum state tomography, the exponent is favorable and allows to perform measurements of the second Rényi entropy for subsystem sizes, which are for instance compatible with the physical examples shown in

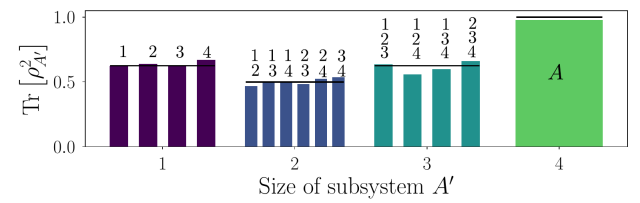


FIG. 4. *Protocol with local unitaries.* Purity of all (sub-)systems $A' \subseteq A$ measured simultaneously using local unitaries with $N_U = 2N_M = 100$. The numbers above the bars refer to the indices $i = 1, \dots, L$ contained in A' , the green bar to $A' = A$. The black lines indicate the exact value.

Fig. 1.

Application to physical examples. – We conclude our discussion by showing how the protocol [c.f. Fig. 1(a)] can be used to investigate entanglement properties of quantum many-body states $|\psi\rangle$. As our first example, we demonstrate in Fig. 1(b) the *measurement of an area law* in a 2D Heisenberg model. We consider a system \mathcal{S} prepared in the $S_z = 0$ ground state $|\psi\rangle$ of H_h on an 8×8 square lattice, obtained numerically by DMRG. For rectangular partitions A with size $L = L_x L_y$ placed at the center of the system, we estimate the second Rényi entropy $S^{(2)}(\rho_A)$ of the reduced density matrices $\rho_A = \text{Tr}_{\mathcal{S} \setminus A} [|\psi\rangle\langle\psi|]$ as a function of the partition boundary $\partial A = 2(L_x + L_y - 2)$. We observe that the estimated Rényi entropy converges to the area law result [43] with increasing number of quenches η . Note that we have used here a finite number of unitaries $N_U = 100$, and a finite number of measurements $N_M = 100$. As our second example, Fig. 1(c) shows for a 1D Bose Hubbard model the *entanglement growth in the many-body localized (MBL) phase* [69, 70], with details on the model and parameters summarized in Ref. [48]. According to Fig. 1(c), the estimated second order Rényi entropy as a function of time clearly allows to distinguish MBL from Anderson localization.

Protocol based on local unitaries. – The measurement scheme described above relies on global entangling unitaries acting on the entire Hilbert space. As an alternative, we can also use *local unitaries*, which act individually on local constituents $i = 1, \dots, L$ (e.g. spins) of A . Here, the unitary U_A is given as a product $U_A = u_1 \otimes \dots \otimes u_L$ where each u_i is independently drawn from a unitary 2-design in the local Hilbert space of dimension d . In the case of a spin system, the u_i can be written as random single spin rotation on the Bloch sphere. The measurement step of the protocol is identical to the one described above for global unitaries. For a measurement outcome $\mathbf{s} = (s_i)_{i=1, \dots, L}$ in a fixed local basis, we compute the statistical moments $\langle P(\mathbf{s})^n \rangle$. We find $\langle P(\mathbf{s}) \rangle = 1/d^L$ [71] and, using the 2-design properties of u_i ,

$$\langle P(\mathbf{s})^2 \rangle = \frac{\sum_{A' \subseteq A} \text{Tr}(\rho_{A'}^2)}{d^L (d+1)^L}. \quad (6)$$

Here, we sum over all subsystems $A' \subseteq A$, including the empty subsystem for which we define $\text{Tr}[\rho_\emptyset^2] \equiv 1$. Since the unitaries act only locally, Eq. (6) holds for each subsystem A' . This allows to reconstruct recursively all purities $\text{Tr}(\rho_{A'}^2)$ for $A' \subseteq A$. Local unitaries allow thus to infer more information from the measurement than global unitaries. This is illustrated in Fig. 4 for $L = 4$ spins initialized in the W -state. We note however, that due to the recursive reconstruction of the purities from Eq. (6), this protocol is more prone to statistical errors [48].

Conclusion and Outlook – The presented protocol allows the measurement of Rényi entropies based on single copies in existing AMO setups: for example, to obtain the purity of a quantum state ρ_A corresponding to a partition A with $L = 14$ spins, as part of an arbitrarily large many-body system, one needs for an accuracy of $\sim 5\%$ $N_M = 500$ measurements, and averaging over $N_U = 100$ unitaries. In an Ising model with $L = 14$ spins, the re-

quired time for the measurement protocol is $JT_{\text{tot}} \sim 25$. While we have focused on measurement of second order Rényi entropies, higher order entropies are also accessible although with increasing statistical errors [48], which provides an interesting perspective to extend the protocol to von Neumann entropies, or the entanglement spectrum [72–74].

We thank the M. Lukin, M. Greiner, M. Hafezi group members, and J. Eisert, C. Roos, P. Jurcevic, G. Pagano, W. Lechner, M. Baranov, H. Pichler, P. Hauke, M. Łacki, and D. Hangleiter for discussions. The DMRG and exact diagonalization simulations were performed using the ITensor library (<http://itensor.org>) and QuTiP [75], respectively. Work in Innsbruck is supported by the ERC Synergy Grant UQUAM and the SFB FoQuS (FWF Project No. F4016-N23). JJC acknowledges support from the ERC grant QUENOCOBA.

[1] I. Bloch, J. Dalibard, and S. Nascimbène, *Nat. Phys.* **8**, 267 (2012).

[2] A. Browaeys, D. Barredo, and T. Lahaye, *J. Phys. B At. Mol. Opt. Phys.* **49**, 152001 (2016).

[3] R. Blatt and C. F. Roos, *Nat. Phys.* **8**, 277 (2012).

[4] S. Murmann, A. Bergschneider, V. M. Klinkhamer, G. Zürn, T. Lompe, and S. Jochim, *Phys. Rev. Lett.* **114**, 080402 (2015).

[5] E. Haller, J. Hudson, A. Kelly, D. A. Cotta, B. Peaudecerf, G. D. Bruce, and S. Kuhr, *Nat. Phys.* **11**, 738 (2015).

[6] D. Greif, M. F. Parsons, A. Mazurenko, C. S. Chiu, S. Blatt, F. Huber, G. Ji, and M. Greiner, *Science* (80-.) **351**, 953 (2016).

[7] M. Boll, T. A. Hilker, G. Salomon, A. Omran, J. Nespolo, L. Pollet, I. Bloch, and C. Gross, *Science* (80-.) **353**, 1257 (2016).

[8] L. W. Cheuk, M. A. Nichols, K. R. Lawrence, M. Okan, H. Zhang, E. Khatami, N. Trivedi, T. Paiva, M. Rigol, and M. W. Zwierlein, *Science* (80-.) **353**, 1260 (2016).

[9] H. Labuhn, D. Barredo, S. Ravets, S. de Léséleuc, T. Macrì, T. Lahaye, and A. Browaeys, *Nature* **534**, 667 (2016).

[10] J. Zeiher, J.-y. Choi, A. Rubio-Abadal, T. Pohl, R. M. W. van Bijnen, I. Bloch, and C. Gross, [arXiv:1705.08372](https://arxiv.org/abs/1705.08372).

[11] H. Bernien, S. Schwartz, A. Keesling, H. Levine, A. Omran, H. Pichler, S. Choi, A. S. Zibrov, M. Endres, M. Greiner, V. Vuletić, and M. D. Lukin, [arXiv:1707.04344](https://arxiv.org/abs/1707.04344).

[12] P. Jurcevic, H. Shen, P. Hauke, C. Maier, T. Brydges, C. Hempel, B. P. Lanyon, M. Heyl, R. Blatt, and C. F. Roos, *Phys. Rev. Lett.* **119**, 080501 (2017).

[13] J. Zhang, G. Pagano, P. W. Hess, A. Kyprianidis, P. Becker, H. Kaplan, A. V. Gorshkov, Z. X. Gong, and C. Monroe, [arXiv:1708.01044](https://arxiv.org/abs/1708.01044).

[14] S. Kuhr, *Natl. Sci. Rev.* **3**, 170 (2016).

[15] J. Eisert, M. Cramer, and M. B. Plenio, *Rev. Mod. Phys.* **82**, 277 (2010).

[16] S. Boixo, S. V. Isakov, V. N. Smelyanskiy, R. Babbush, N. Ding, Z. Jiang, M. J. Bremner, J. M. Martinis, and H. Neven, [arXiv:1608.00263](https://arxiv.org/abs/1608.00263).

[17] J. Bermejo-Vega, D. Hangleiter, M. Schwarz, R. Raussendorf, and J. Eisert, [arXiv:1703.00466](https://arxiv.org/abs/1703.00466).

[18] X. Gao, S. T. Wang, and L. M. Duan, *Phys. Rev. Lett.* **118**, 1 (2017).

[19] M. J. Bremner, A. Montanaro, and D. J. Shepherd, *Quantum* **1**, 8 (2017).

[20] S. Boixo, V. N. Smelyanskiy, and H. Neven, [arXiv:1708.01875](https://arxiv.org/abs/1708.01875).

[21] S. J. van Enk and C. W. J. Beenakker, *Phys. Rev. Lett.* **108**, 110503 (2012).

[22] A. J. Daley, H. Pichler, J. Schachenmayer, and P. Zoller, *Phys. Rev. Lett.* **109**, 020505 (2012).

[23] D. A. Abanin and E. Demler, *Phys. Rev. Lett.* **109**, 020504 (2012).

[24] R. Islam, R. Ma, P. M. Preiss, M. Eric Tai, A. Lukin, M. Rispoli, and M. Greiner, *Nature* **528**, 77 (2015).

[25] A. M. Kaufman, M. E. Tai, A. Lukin, M. Rispoli, R. Schittko, P. M. Preiss, and M. Greiner, *Science* (80-.) **353**, 794 (2016).

[26] A. a. Houck, H. E. Türeci, and J. Koch, *Nat. Phys.* **8**, 292 (2012).

[27] J. Cai, A. Retzker, F. Jelezko, and M. B. Plenio, *Nat. Phys.* **9**, 168 (2013).

[28] D. Gross, Y.-k. Liu, S. T. Flammia, S. Becker, and J. Eisert, *Phys. Rev. Lett.* **105**, 150401 (2010).

[29] M. Cramer, M. B. Plenio, S. T. Flammia, R. Somma, D. Gross, S. D. Bartlett, O. Landon-Cardinal, D. Poulin, and Y.-K. Liu, *Nat. Commun.* **1**, 149 (2010).

[30] B. P. Lanyon, C. Maier, M. Holzapfel, T. Baumgratz, C. Hempel, P. Jurcevic, I. Dhand, A. S. Buyskikh, A. J. Daley, M. Cramer, M. B. Plenio, R. Blatt, and C. F. Roos, [arXiv:1612.08000](https://arxiv.org/abs/1612.08000).

[31] R. Oliveira, O. C. O. Dahlsten, and M. B. Plenio, *Phys. Rev. Lett.* **98**, 1 (2007).

[32] M. Žnidarič, *Phys. Rev. A* **78**, 032324 (2008).

[33] We can thus extract $S^{(2)}(\rho_A)$ from any state \mathbf{s} . This implies that, by averaging the estimations of $S^{(2)}(\rho_A)$ obtained from different states \mathbf{s} , statistical errors can be reduced by a factor $\sim 1/\sqrt{N_A}$ (c.f below).

[34] D. Gross, K. Audenaert, and J. Eisert, *J. Math. Phys.* **48**, 52104 (2007).

[35] A. Roy and A. J. Scott, *Des. Codes Cryptogr.* **53**, 13 (2009).

[36] L. D'Alessio and A. Polkovnikov, *Ann. Phys. (N. Y.)* **333**, 19 (2013).

[37] L. D'Alessio and M. Rigol, *Phys. Rev. X* **4**, 1 (2014).

[38] P. Ponte, A. Chandran, Z. Papić, and D. A. Abanin, *Ann. Phys. (N. Y.)* **353**, 196 (2015).

[39] S. Gopalakrishnan, M. Knap, and E. Demler, *Phys. Rev. B* **94**, 094201 (2016).

[40] F. Machado, G. D. Meyer, D. V. Else, C. Nayak, and N. Y. Yao, [arXiv:1708.01620](https://arxiv.org/abs/1708.01620).

[41] P. Bordia, H. Lüschen, U. Schneider, M. Knap, and I. Bloch, *Nat. Phys.* **13**, 460 (2017).

[42] F. Haake, *Quantum Signatures of Chaos*, Vol. 54 (Springer, 2010).

[43] H. F. Song, N. Laflorencie, S. Rachel, and K. Le Hur, *Phys. Rev. B* **83**, 224410 (2011).

[44] D. M. Basko, I. L. Aleiner, and B. L. Altshuler, *Ann. Phys. (N. Y.)* **321**, 1126 (2006).

[45] R. Nandkishore and D. A. Huse, *Annu. Rev. Condens. Matter Phys.* **6**, 15 (2015).

[46] E. Altman and R. Vosk, *Annu. Rev. Condens. Matter Phys.* **6**, 383 (2015).

[47] We note that for each projective measurement we apply the same random unitary U_A to estimate the probabilities $\langle P(s_{N,S_z}) \rangle$, i.e. the same series of random quenches.

[48] See *Supplementary Material*, which includes Refs. [47-56].

[49] B. Collins and P. Śniady, *Commun. Math. Phys.* **264**, 773 (2006).

[50] Z. Puchała and J. Miszczak, *Bull. Polish Acad. Sci. Tech. Sci.* **65**, 17 (2017).

[51] L. Isserlis, *Biometrika* **12**, 134 (1918).

[52] M. Bona, *Combinatorics of Permutations, Second Edition*, Discrete Mathematics and Its Applications (CRC Press, 2016).

[53] M. Ohliger, V. Nesme, and J. Eisert, *New J. Phys.* **15**, 015024 (2013).

[54] J. Preskill, “Lectures Notes on Quantum Computation,” (2001).

[55] T. Guhr, A. Müller-Groeling, and H. A. Weidenmüller, *Phys. Rep.* **299**, 189 (1998).

[56] N. Ullah and C. E. Porter, *Phys. Rev.* **132**, 948 (1963).

[57] F. Mezzadri, *Not. Am. Math. Soc.* **54**, 592 (2006).

[58] G. P. Wadsworth and J. G. Bryan, *Introduction to Probability and Random Variables*, A Wiley publication in mathematical statistics (McGraw-Hill, 1960).

[59] C. Dankert, R. Cleve, J. Emerson, and E. Livine, *Phys. Rev. A* **80**, 012304 (2009).

[60] F. Brandão, A. W. Harrow, and M. Horodecki, *Commun. Math. Phys.* **346**, 397 (2016).

[61] A. V. Gorshkov, S. R. Manmana, G. Chen, E. Demler, M. D. Lukin, and A. M. Rey, *Phys. Rev. A* **84**, 033619 (2011).

[62] D. Porras and J. I. Cirac, *Phys. Rev. Lett.* **92**, 207901 (2004).

[63] The creation of random unitaries is also possible using quasi-random disorder created by Aubry-André potentials [76]. For the investigated system sizes, we find that the required time is similar to the case of true random disorder.

[64] Note that the estimated purity can be larger than one for $T_{\text{tot}} \rightarrow 0$, corresponding to $U_A \rightarrow \mathbf{1}$.

[65] P. Facchi, S. Montangero, R. Fazio, and S. Pascazio, *Phys. Rev. A* **71**, 060306 (2005).

[66] A. Nahum, J. Ruhman, S. Vijay, and J. Haah, *Phys. Rev. X* **7**, 031016 (2017).

[67] Note that this is in contrast to exact 2-designs [34] where the error vanishes completely for a finite (but large) set of unitaries.

[68] S. M. Blinder, *Guide to Essential Math: A Review for Physics, Chemistry and Engineering Students* (Elsevier, 2013).

[69] J. H. Bardarson, F. Pollmann, and J. E. Moore, *Phys. Rev. Lett.* **109**, 1 (2012).

[70] M. Serbyn, Z. Papić, and D. A. Abanin, *Phys. Rev. Lett.* **110**, 260601 (2013).

[71] This means that the local unitaries U_A form a 1-design.

[72] H. Li and F. D. M. Haldane, *Phys. Rev. Lett.* **101**, 1 (2008).

[73] H. Pichler, G. Zhu, A. Seif, P. Zoller, and M. Hafezi, *Phys. Rev. X* **6**, 041033 (2016).

[74] M. Dalmonte, B. Vermersch, and P. Zoller, [arXiv:1707.04455](https://arxiv.org/abs/1707.04455).

[75] J. R. Johansson, P. D. Nation, and F. Nori, *Comput. Phys. Commun.* **184**, 1234 (2013).

[76] S. Aubry and G. André, *Ann. Isr. Phys.* , 133 (1980).

[77] We observed that the convergence to 2-designs obeys the same scalings for mixed states.

Appendix A: Details on the measurement protocol

Here we present the derivation of Eqs. (4) and (5) of the main text (MT), which relate correlations of random measurements performed on a (sub-) system A with functionals $\text{Tr}_A [\rho_A^n]$ of the (reduced) density matrix ρ_A . Thereby, we extend the framework presented in [21] to incorporate random unitaries created via quench dynamics with symmetry constraints, and random measurements of arbitrary observables. Furthermore, we give explicit expressions for arbitrary $n \in \mathbb{N}$.

We note that a measurement of n -th order Rényi entropy involves only correlations of random unitaries up to order n . If one is interested in the estimation of Rényi entropies up n -th order only, it is hence sufficient to use in the following, instead of the full Circular Unitary Ensemble (CUE), a unitary n -design [34].

1. Purity from random measurements of arbitrary observables

Rényi entropies associated with a (reduced) density matrix ρ_A defined in Hilbert space with dimension \mathcal{N}_A are interfered from correlations of output probabilities of random measurements. On a quantum computer, a random measurement can be realized using a random unitary $U_A \in \text{CUE}(\mathcal{N}_A)$, generated by a random gate sequence and applied to $\rho_A \rightarrow U_A \rho_A U_A^\dagger$, and a subsequent measurement in a fixed (computational) basis [21]. In an atomic Hubbard or spin model [see MT and below],

we generate U_A as time evolution as sequence of random quenches. Due to symmetries of the quench Hamiltonian evolution, U_A decomposes into blocks, $U_A = \bigoplus_{\alpha} U_A^{\alpha}$, labeled by quantum numbers $\alpha = (\alpha_1, \dots, \alpha_q)$ which correspond to a set of conserved quantities Q_p ($p = 1, \dots, q$), with $[U_A, Q_p] = 0$. The (reduced) states $\rho_A = \bigoplus_{\alpha} \rho_A^{\alpha}$ have the same block structure, due to the same conservation laws. The symmetries for the FH are discussed below.

In the following, we assume that $U_A^{\alpha} \in \text{CUE}(\mathcal{N}_A^{(\alpha)})$ where $\mathcal{N}_A^{(\alpha)}$ denotes the dimension of the sector α . To realize a random measurement, U_A is then first applied to $\rho_A = \bigoplus_{\alpha} \rho_A^{\alpha} \rightarrow \bigoplus_{\alpha} U_A^{\alpha} \rho_A^{\alpha} U_A^{\alpha\dagger}$. This is followed by a measurement of an observable \mathcal{O} . We assume that measurement of this observable does not mix these sectors, i.e. must resolve the quantum numbers α ($[Q_p, \mathcal{O}] = 0$ for all $p = 1, \dots, q$), but can be arbitrary otherwise. We denote the outcome of a corresponding measurement with \mathbf{s}_{α} , where α are the associated the quantum numbers, and the corresponding projector with $\mathcal{P}_{\mathbf{s}_{\alpha}}^{\mathcal{O}}$. For a fixed random unitary U_A , the probability $P(\mathbf{s}_{\alpha})$ to obtain a measurement outcome \mathbf{s}_{α} is given by $P(\mathbf{s}_{\alpha}) = \text{Tr}_A [U_A \rho_A U_A^{\dagger} \mathcal{P}_{\mathbf{s}_{\alpha}}^{\mathcal{O}}]$. Using the Weingarten calculus for the moments of the Haar measure of the unitary group [49, 50], one finds from an average over these outcome probabilities of random measurements (over the random unitary ensemble)

$$\langle P(\mathbf{s}_{\alpha}) \rangle = \frac{\text{Tr} [\mathcal{P}_{\mathbf{s}_{\alpha}}^{\mathcal{O}}] \text{Tr} [\rho_A^{(\alpha)}]}{\mathcal{N}_A^{(\alpha)}} \quad (\text{A1})$$

$$\begin{aligned} \langle P(\mathbf{s}_{\alpha})^2 \rangle &= \frac{\text{Tr} [\mathcal{P}_{\mathbf{s}_{\alpha}}^{\mathcal{O}}]^2 \text{Tr} [\rho_A^{(\alpha)}]^2 + \text{Tr} [\mathcal{P}_{\mathbf{s}_{\alpha}}^{\mathcal{O}}] \text{Tr} [\rho_A^{(\alpha)2}]}{\mathcal{N}_A^{(\alpha)2} - 1} \\ &\quad - \frac{\text{Tr} [\mathcal{P}_{\mathbf{s}_{\alpha}}^{\mathcal{O}}]^2 \text{Tr} [\rho_A^{(\alpha)2}] + \text{Tr} [\mathcal{P}_{\mathbf{s}_{\alpha}}^{\mathcal{O}}] \text{Tr} [\rho_A^{(\alpha)}]^2}{\mathcal{N}_A^{(\alpha)}(\mathcal{N}_A^{(\alpha)2} - 1)}. \end{aligned} \quad (\text{A2})$$

Here, $\langle \dots \rangle$ denotes the ensemble average over the CUE (or more generally a unitary 2-design). These equations can be solved to determine $\text{Tr} [\rho_A^{(\alpha)2}]$, and by summation over all sectors $\text{Tr} [\rho_A^2] = \sum_{\alpha} \text{Tr} [\rho_A^{(\alpha)2}]$.

For the Fermi Hubbard (FH) model (see MT) the conserved quantities are the total magnetization S_z and total particle number N , i.e $\alpha = S_z, N$. An observable resolving S_z and N is the spin-resolved measurement of the local particle number with a quantum gas microscope. Given an outcome $\mathbf{s}_{N, S_z} = (\mathbf{n}_{\uparrow}, \mathbf{n}_{\downarrow})$ of such a measurement, we find $S_z = \sum_{\mathbf{i}} \mathbf{n}_{\uparrow, \mathbf{i}} - \mathbf{n}_{\downarrow, \mathbf{i}}$ and $N = \sum_{\mathbf{i}} \mathbf{n}_{\uparrow, \mathbf{i}} + \mathbf{n}_{\downarrow, \mathbf{i}}$. The projectors are $\mathcal{P}_{\mathbf{s}_{N, S_z}}^{\mathcal{O}} = |\mathbf{n}_{\uparrow}, \mathbf{n}_{\downarrow}\rangle \langle \mathbf{n}_{\uparrow}, \mathbf{n}_{\downarrow}|$ with the Fock states $|\mathbf{n}_{\uparrow}, \mathbf{n}_{\downarrow}\rangle$ and $\text{Tr} [\mathcal{P}_{\mathbf{s}_{N, S_z}}^{\mathcal{O}}] = 1$. Eqs. (A1) and (A2) then reduce to Eqs. (4) and (5) of the MT.

2. Higher order functionals

We describe now the estimation of higher order functionals $\text{Tr} [\rho_A^n]$, related to averages of higher order polynomials of outcome probabilities $\langle P(\mathbf{s}_{\alpha})^n \rangle$. We adapt definitions and notations from the previous subsection. For measurements of observables with $\text{Tr} [\mathcal{P}_{\mathbf{s}_{\alpha}}^{\mathcal{O}}] > 1$, the ensemble averages $\langle P(\mathbf{s}_{\alpha})^n \rangle$ ($n \in \mathbb{N}$) can be calculated order by order in n using the Weingarten calculus [49, 50]. An explicit formula can be given for direct measurements of occupation probabilities of basis states ($\text{Tr} [\mathcal{P}_{\mathbf{s}_{\alpha}}^{\mathcal{O}}] = 1$) based on Isserlis' theorem [21, 51]. The evaluation of $\langle P(\mathbf{s}_{\alpha})^n \rangle$ reduces then to the counting of permutations in the symmetric group S_n . One finds

$$\langle P(\mathbf{s}_{\alpha})^n \rangle \stackrel{\text{Tr} [\mathcal{P}_{\mathbf{s}_{\alpha}}^{\mathcal{O}}] = 1}{=} \frac{1}{D_n} \sum_{\substack{b_1, \dots, b_n \in \mathbb{N}_0 \\ \text{with} \\ \sum_{l=1}^n l b_l = n}} C_{b_1, \dots, b_n} \prod_{k=1}^n \text{Tr} [\rho_A^{(\alpha)k}]^{b_k} \quad (\text{A3})$$

where $D_n = \prod_{i=0}^{n-1} (\mathcal{N}_A^{(\alpha)} + i)$. C_{b_1, \dots, b_n} denotes the number of permutations $\pi \in S_n$ with $\text{typ}(\pi) = 1^{b_1} 2^{b_2} \dots n^{b_n}$ and is given by [52]

$$C_{b_1, \dots, b_n} = \frac{n!}{b_1! \cdot b_2! \cdot \dots \cdot b_n! \cdot 1^{b_1} \cdot 2^{b_2} \cdot \dots \cdot n^{b_n}}. \quad (\text{A4})$$

Knowing $\text{Tr} [\rho_A^{(\alpha)k}]^{b_k}$ for $k < n$, Eq. (A3) can be solved to obtain $\text{Tr} [\rho_A^{(\alpha)n}]$. By summation over all sectors, one finds $\text{Tr} [\rho_A^n] = \sum_{\alpha} \text{Tr} [\rho_A^{(\alpha)n}]$.

Appendix B: Generation of unitaries in the 1D and 2D Heisenberg models

In this section, we complement the study of the convergence to 2-designs for the Heisenberg model, as presented in the MT. We first discuss the optimization of the disorder strength δ and then present the possibility to create 2-designs from a single disorder pattern.

The optimization of random quenches with respect to δ is shown in Fig. 5 (a) for the antiferromagnetic state $|\psi_{\text{AF}}\rangle$, $(L_x, L_y) = (8, 1)$, and different times $T_{\text{tot}} = \eta/J$. The error of the estimated purity is minimal around $\delta \sim J$. Overall, we remark that the convergence to CUE is favored when all the relevant frequencies associated with the quenches are of the same order of magnitude (here $J \approx \delta \approx 1/T$).

For simplicity, we discuss in the MT the case where for each quench j , the applied disorder pattern δ_i^j is not correlated with the previous realizations $j' < j$. This implies that the source of disorder (as implemented for instance with spatial light modulators (SLM) or speckle patterns in AMO systems) is dynamically reconfigurable. In Fig. 5(b), we show that random unitaries converging

to 2-designs can be also realized using a single disorder pattern δ_i , which is drawn from a normal distribution of standard deviation $\delta = J$, and applied every second quench: $\delta_i^j = \delta_i \text{mod}(j, 2)$, provided the quench times $T \rightarrow T_j$ depend on j and are random (here drawn for a uniform distribution in the interval $[0, 2J^{-1}]$).

Note that in the case of a constant quench time $JT_j = 1$ (blue lines), corresponding to a Floquet system of period $2T$, the error remains large ($\sim 10^{-1}$) and does not depend on the number of unitaries $N_U = 100, 500$, i.e. is not due to statistical errors. We attribute this to the slow thermalization dynamics of Floquet systems [37, 40], occurring at $JT_{\text{tot}} \gg 1$ (which is not visible in Fig. 5).

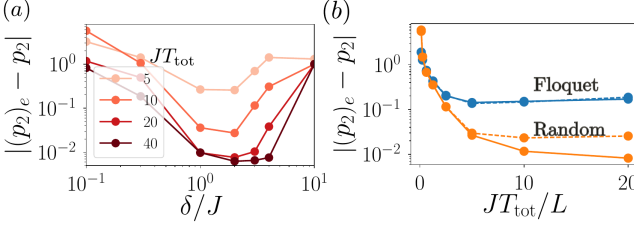


FIG. 5. *Convergence to a unitary 2-design in the 2D Heisenberg model.* We consider an antiferromagnetic state, $L_x, L_y = 8, 1$, $N_U = 500$, and $N_M = \infty$. (a) Influence of the disorder strength δ for different T_{tot} , showing an optimum at $\delta \approx J$. (b) Convergence to the CUE with a single disorder pattern δ_j and random times T_j . The dashed lines show the error for $N_U = 100$.

Appendix C: Generation of unitaries in the 2D Fermi-Hubbard model

We present here a numerical study of the generation of 2-designs in the Fermi-Hubbard (FH) model. Our approach is identical to the case of the Heisenberg model and Quantum Ising models presented in Fig. 2 of the MT. We choose test states ρ_A and compare the estimated purity $(p_2)_e$ with the exact purity p_2 . For simplicity, we consider density matrices ρ_A as pure states $\rho_A = |\psi_{N,S_z}\rangle \langle \psi_{N,S_z}|$ of a single quantum number sector (N, S_z) [77]. For the examples presented in Fig. 6, we use

$$\begin{aligned} |\psi_{1,1}\rangle &= (c_{\mathbf{i}=(1,1),\uparrow}^\dagger + c_{(L_x, L_y),\uparrow}^\dagger)/\sqrt{2}|V\rangle \\ |\psi_{2,0}\rangle &= (c_{(1,1),\downarrow}^\dagger c_{(L_x, L_y),\uparrow}^\dagger + c_{(L_x, 1),\downarrow}^\dagger c_{(1, L_y),\uparrow}^\dagger)/\sqrt{2}|V\rangle \\ |\psi_{2,2}\rangle &= (c_{(1,1),\uparrow}^\dagger c_{(2,1),\uparrow}^\dagger + c_{(L_x-1, L_y),\uparrow}^\dagger c_{(L_x, L_y),\uparrow}^\dagger)/\sqrt{2}|V\rangle, \end{aligned} \quad (C1)$$

with $|V\rangle$ the vacuum state. We consider spin-dependent disorder potentials with $\Delta_{\mathbf{i},\uparrow} = 2\Delta_{\mathbf{i},\downarrow}$, which however differ only by a global prefactor. $\Delta_{\mathbf{i},\downarrow}$ is drawn from a normal distribution of standard deviation δ .

As in the Heisenberg model (derived from the FH in the limit $t_F \ll U$ and half filling), the error of the estimated purity, shown in Fig. 6(a) for $(N, S_z) = (2, 0)$

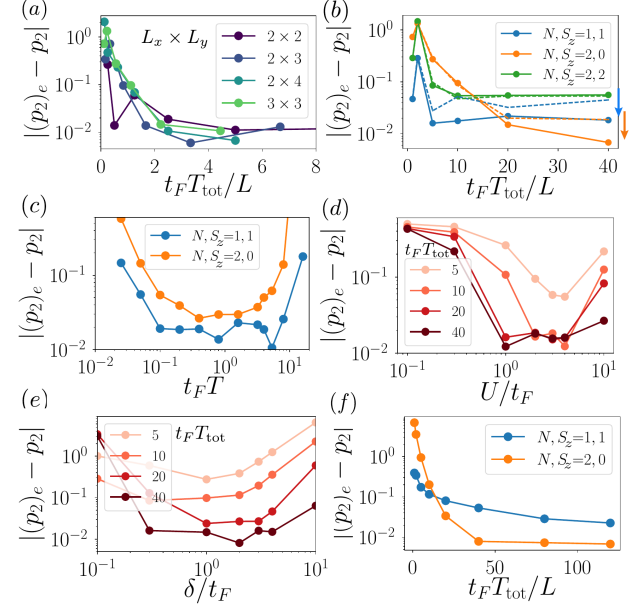


FIG. 6. *Creation of random unitaries in the 2D Fermi Hubbard model.* (a) The average error of the estimated purity of $|\psi_{2,0}\rangle$ is shown as a function of η and for different partition sizes L_x, L_y . The convergence to a unitary 2-design is exponential with scaling parameter $t_F T_{\text{tot}}/L$. (b) The error is shown for $N_U = 100$ (dashed) and $N_U = 500$ (solid lines) and for different sectors. For $N, S_z = 2, 2$, this plateau is due to the non-interacting character of the sector (see text). (c) For $T_{\text{tot}} = 16/t_F$, error as a function of T , with an optimum at $t_F T \approx 1$. (d)-(e) Influence of the Hamiltonian parameters U and δ on the error of the estimated purity for $|\psi_{2,0}\rangle$. (f) Convergence to a unitary 2-design with a single disorder pattern and random gate times T_j . Unless stated otherwise, $N_U = 500$, $N_M = \infty$, $\delta = U = t_F$, $t_F T = 1$ and $(L_x, L_y) = (3, 3)$.

and for different 2D partitions, decreases exponentially with the preparation time T_{tot} , reaching the statistical error threshold at $t_F T_{\text{tot}} \sim 2L$. In panel (b), we represent the error for different number of unitaries N_U and different quantum number sectors (N, S_z) . Note that the plateau associated with the sector $N = S_z = 2$ does not decrease with N_U and is thus not due to statistical errors. It originates from the fact that the FH model is a non-interacting model for this specific sector where all fermions have the same spin and thus ‘entangling’ random unitaries cannot be created. However, for the physical examples we are interested in [c.f in Fig. 1(b) of the MT], this sector is only marginally populated leading to negligible errors in the estimated purity. In panel (c), the error of the purity is shown as a function of the quench time T , while keeping the total time $T_{\text{tot}} = 16/t_F$ fixed. As in the Heisenberg model, the optimal quench time $T \sim t_F^{-1} \sim 1$ is of the order of the tunnelling time. In panel (d-e), we show the optimization of the other quench parameters: here the interaction U and disorder δ strengths.

As in Fig. 5(b), we show in Fig. 6(f) the error of the purity estimated with random unitaries, which are created using a single disorder pattern which is switched on and off after random times T_j , drawn from a uniform distribution in $[0, 2/t_F]$. Note that convergence to a unitary 2-design requires a larger number of quenches compared to the case of multiple disorder patterns [c.f panel (a)].

Appendix D: Generation of random unitaries in the 1D Quantum Ising model

Here, we give details on the generation of random unitaries in the Quantum Ising model, as realized with trapped ions or Rydberg atoms, corresponding to the results shown in Fig. 2 (e-f) of the MT. Additionally we investigate the creation of higher order designs $n = 2, 3, 4$, enabling the estimation of higher order Renyi entropies.

1. Generation of approximate 2-designs

As in the FH and Heisenberg models, random unitaries are generated using a series of random quenches. We consider a uni-dimensional chain of L spins. The quenches are governed by Hamiltonians H_A^j ($j = 1, \dots, \eta$), with

$$H_A^j = \sum_{i \in A} \frac{C_\alpha}{a^\alpha |i - l|^\alpha} \sigma_i^u \sigma_l^u + \Omega \sum_{i \in A} \sigma_i^x + \sum_{i \in A} \delta_i^j \sigma_i^x \text{D1})$$

with a the lattice spacing and $u = x$, $\alpha = 1.5$ ($u = z$, $\alpha = 6$) for the trapped ions (Rydberg atoms) case, respectively. The disorder potentials are drawn from a normal distribution with standard deviation δ . For Fig. 2 (e-f), we have chosen $\delta = \Omega = J$, with $J \equiv C_\alpha/a^\alpha$. The quench time is fixed $T = 1/\Omega$ and we use here an anti-ferromagnetic test state (we observe the same scalings of errors for other test states).

We find that, as in the Heisenberg model, the error of the estimated purity decreases exponentially with $JT_{\text{tot}}/L = \eta/L$, indicating the creation of approximate 2-designs after a time which scales linearly with respect to the partition size L . Moreover, we remark that 2-designs can also be created (i) in a ‘digital’ approach where the disorder patterns and the interactions (the transverse field Ω) are applied only on even (resp. odd) quenches j , and (ii) without transverse field $\Omega = 0$. Note that in the case (ii) the parity $\text{mod}(S_z, 2)$ is a conserved quantum number.

2. Generation of higher-order designs

In Fig. 7, we show the convergence to higher order designs in the Quantum Ising model. Using the same parameters and test state as in Fig. 2 of the MT, we observe an exponential decrease of the error of an estimate $(p_n)_e$ ($n = 2, 3, 4$) with the number of quenches

η . However, the absolute error and hence the number of random quenches and number of random unitaries and measurements (cf. App. H) to reach an approximate n -design increases with n , as in random circuits [53]. For low order designs $n = 2, 3, 4, \dots$, the time required to create approximate n -designs are however still compatible with AMO experimental timescales.

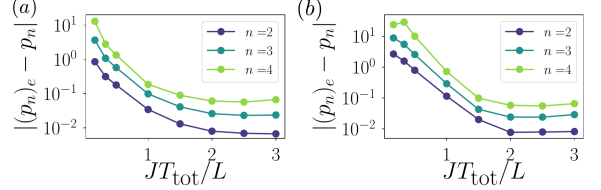


FIG. 7. *Creation of higher order n -designs in the 1D Quantum Ising model.* Convergence to $n = 2, 3, 4$ designs for random quenches in long range Quantum Ising models for $L = 6$ and same parameters as in Fig. 2 of the MT. In panel (a), we show the Rydberg case $\alpha = 1.5$, $u = x$, in panel (b) the trapped ions case $\alpha = 6$, $u = z$.

Appendix E: Details on the Bose-Hubbard simulation

In this section, we give additional details on Fig. 1(c) of the MT, corresponding to the simulation of the measurement of the MBL entanglement growth. The BH Hamiltonian governing its dynamics is given by

$$H_B = -J \sum_{i \in S} (a_{i+1}^\dagger a_i + \text{h.c.}) + \frac{U}{2} \sum_{i \in S} n_i(n_i - 1) + \sum_{i \in S} \Delta_i n_i \quad (\text{E1})$$

with hopping J , onsite interaction U and local disorder potentials Δ_i . Here, a_i (a_i^\dagger) denote bosonic annihilation (creation) operators and $n_i = a_i^\dagger a_i$ the local number operators. We consider a system with $L_S = 10$ sites and $N_S = 5$ particles. We calculate its time evolution, via a Matrix-Product-State (MPS) simulation, for static disorder potentials Δ_i uniformly distributed in $[-10J, 10J]$ in the Anderson-localized ($U/J = 0$) or many-body localized phase ($U/J = 1$). We then obtain the second order Rényi entropy $S^{(2)}(\rho_A)$, at half partition A , as a function of time t , and averaged over 250 disorder realizations (solid lines).

To simulate the measurement scheme, we apply to ρ_A , which is extracted from the MPS simulation at certain times t , a series ($j = 1, \dots, \eta = 20$) of random quenches governed by $H_A^j = -J \sum_{i \in A} (a_{i+1}^\dagger a_i + \text{h.c.}) + U/2 \sum_{i \in A} n_i(n_i - 1) + \sum_{i \in A} \Delta_i^j n_i$ with (weak) disorder patterns Δ_i^j drawn for each quench from a normal distribution with standard deviation J . The interaction during the random quenches is chosen to be $U = J$. The

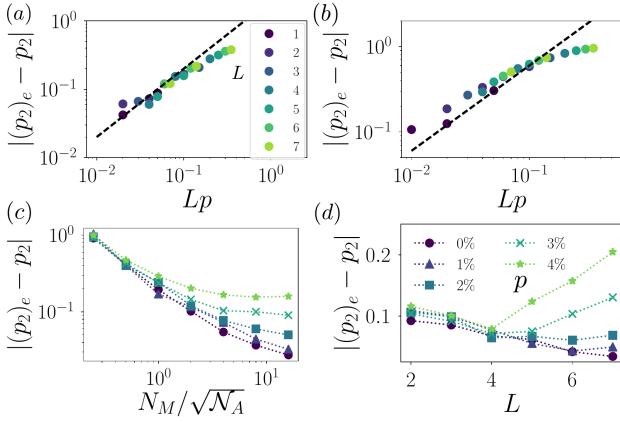


FIG. 8. *Imperfections of the measurement scheme.* (a-b) Decoherence effects in the measurement of Rényi entropies. Relative error of the estimated purity when applying the protocol for a set of $L = 1, \dots, 7$ spins with jump probability $p = 0.01, 0.02, 0.05$, after the dissipative evolution given by Eqs. (F2), (F3). For both dissipative channels, dephasing (a) and depolarizing (b), the error scales linearly with the number of atoms L and the probability p . In panel (a), respectively (b), the black dashed line represents the total jump probability $2Lp$ (resp $6Lp$). For each point represented, we consider one set of $N_U = 500$ random unitaries, drawn from the CUE. (c-d) Error of the estimated purity with imperfectly reproduced disorder patterns (variation of order $p\Delta$ for each projective measurement) created by $\eta = 2L$ quenches of time $T = 1/J$ and disorder strength $\Delta/J = 1$, (c) as a function of N_M for $L = 6$ (d) as a function of L for $N_M = N_A$. For both panels, we consider $N_U = 100$.

corresponding estimated Rényi entropies, represented as circles, clearly enable to distinguish between Anderson- and many-body localized regime.

Appendix F: Imperfections

Our measurement scheme relies on the ability (i) to evolve coherently quantum systems and (ii) to reproduce this evolution with high-fidelity (in order to access observables via projective measurements). Thus one must carefully investigate the sensitivity to decoherence and imperfections (as familiar from atomic quantum simulation [1]). Below, we quantify these requirements and find that they are compatible with current AMO setups.

1. Decoherence

In the MT we estimate the minimum time T_{tot} , which is required to generate approximate 2-designs via random quenches. The goal of this section is to study the effect of decoherence, acting on the system during T_{tot} , on the measurement of purities ($n = 2$ Rényi entropies).

We describe the time evolution of the sub-system A

density matrix via a Markovian master equation

$$\dot{\rho}_A = (\mathcal{L}_D + \mathcal{L}_U) \rho_A, \quad (\text{F1})$$

where \mathcal{L}_D is the Liouvillian corresponding to a Markovian bath and \mathcal{L}_U corresponds to the unitary part of the evolution.

We now assume that the rate γ associated with the decoherence processes are small compared to the frequency scales of the unitary evolution (i.e the eigenvalues of H_A^j) and use a Trotter approximation to describe the final state

$$\rho_A^f = \mathcal{D}\mathcal{U}\mathcal{D}\rho_A, \quad (\text{F2})$$

with the unitary operator $\mathcal{U}(\rho) = U_A \rho U_A^\dagger$ and the Liouvillian evolution operator $\mathcal{D} = e^{\mathcal{L}_D T_{\text{tot}}/2}$. This approximation allows to obtain the first order corrections to ρ_A^f in γT_{tot} , with respect to the ideal unitary case $\gamma = 0$. From Eq. (F2), we notice that decoherence mechanisms affect in this approximation the state of the system before and after the unitary U_A is applied. Note that the first contribution, acting directly on ρ_A , implies that the error cannot be corrected without prior knowledge of the input state.

For our numerical analysis, we consider the dephasing and fully depolarizing channels with Liouvillian operator [54]

$$\mathcal{D} = \prod_{i=1}^L \mathcal{D}_i \quad (\text{F3})$$

$$\mathcal{D}_i(\rho) = (1 - p)\rho + p\sigma_i^z \rho \sigma_i^z \quad (\text{dephasing})$$

$$\mathcal{D}_i(\rho) = (1 - 3p)\rho + p \sum_{\alpha=x,y,z} \sigma_i^\alpha \rho \sigma_i^\alpha \quad (\text{depolarizing}),$$

with $p = \gamma T_{\text{tot}}/2$, where γ is the decoherence rate. This decomposition in terms of Kraus operators is valid in first order in $p \ll 1$. We use a system of L spins $1/2$ and the pure state $\rho_A = |\psi_{\text{ME}}\rangle \langle \psi_{\text{ME}}|$, with $|\psi_{\text{ME}}\rangle = (|\uparrow\rangle^L + |\downarrow\rangle^L)/\sqrt{2}$, which is fragile against both channels. We finally assume that the random quenches generate perfect 2-design and sample unitaries U_A directly from the CUE. The relative error of the estimated purity is shown in Fig. 8(a-b). For the dephasing channel [panel (a)], we notice that the error scales linearly with the decoherence probability p and the number of atoms L . It approximately corresponds to the total probability $2pL$ (shown as dashed lines) of having, in the quantum trajectory picture, a quantum jump. The same observation applies to the depolarizing channel, with total probability $6pL$ [panel (b)].

In summary, decoherence mechanisms lead to a linear scaling of errors with respect to the system size L and the local probability of errors p . Given that for a system size L , the required time to create unitaries is $T_{\text{tot}} \sim L J^{-1}$, where J here refers to the Hamiltonian timescale ($J \rightarrow t_F$ for the FH model). This translates to a condition for the decoherence rate $\gamma \ll J/L^2$, which can be satisfied in current AMO setups with moderate system sizes.

2. Limited reproducibility of generated unitaries

To estimate for a fixed random unitary U_A the probability $P(\mathbf{s})$ of an output \mathbf{s} , a set of $N_M \gg 1$ projective measurements have to be performed on the same state $\rho_A^f = U_A \rho_A U_A^\dagger$. Hence, for each measurement, the same random unitary U_A has to be created, via the same random quench dynamics. Here, we discuss the influence of imperfect reproducibility of the random unitaries (i.e. the disorder patterns implementing random quenches) on statistical errors.

To be specific, we consider the Quantum Ising model with $u = z$ and $\alpha = 6$ (Rydberg atoms), and $\rho_A = |\uparrow \dots \uparrow\rangle \langle \uparrow \dots \uparrow|$ as test state. To create a random unitary U_A , η disorder patterns δ_i^j ($i = 1, \dots, L$) are drawn from a normal distribution with standard deviation $\Delta = \Omega = C_6/a^6$ where a is the lattice spacing.

We now assume that for each of the $m = 1, \dots, N_M$ projective measurements, these disorder patterns, and thus the random unitary U_A , are only imperfectly reproduced. To simulate this numerically, we add for each measurement additional disorder patterns $\tilde{\delta}_i^{j,m}$ to H_A^j drawn from a normal distribution with standard deviation $p\Delta$ ($p \ll 1$). The resulting statistical error of the purity [shown in Fig. 8, panel (c)], does not decrease as a function of the number of measurements N_M towards $1/\sqrt{N_U N_A}$ but converges to a higher value, set by the size of the error p . For $N_M = N_A$ measurements and $\eta = 2L$, we observe that the error increases approximately linearly with L [panel (d)], due to the larger number $\eta \sim L$ of quenches to create a random unitary.

In summary, assuming a reproducibility of disorder patterns with an error p of a few percent, and moderate system sizes, the estimation of the purity can be obtained with a reasonable accuracy.

Appendix G: Random unitaries and many-body quantum chaos

In the MT, we use the error of the estimated purity $|(p_2)_e - p_2|$ of various states to test the convergence of random unitaries ensembles. In this section, we compare this quantity to other tools certifying random unitaries based on random matrix theory [55] and quantum chaos [42]. We consider the inverse participation ratio (IPR) and the statistics of the eigenvalues (eigenphases) of the created unitary operators. In particular, we identify using these tools the transition from many-body localized ($\eta = 1$) to chaotic dynamics ($\eta \gg 1$).

Given a unitary U_A with eigenstates $|\phi_\nu\rangle$ and eigenvalues $e^{i\theta_\nu}$ ($\nu = 1, \dots, N_A$), the IPR of a state ρ_A

$$\text{IPR}(\rho_A) = \sum_{\nu=1}^{N_A} \text{Tr} [\rho_A |\phi_\nu\rangle \langle \phi_\nu|]^2 \quad (\text{G1})$$

is a measure for the spreading (delocalization) of ρ_A in the eigenbasis of U_A . It is maximal for an eigenstate of

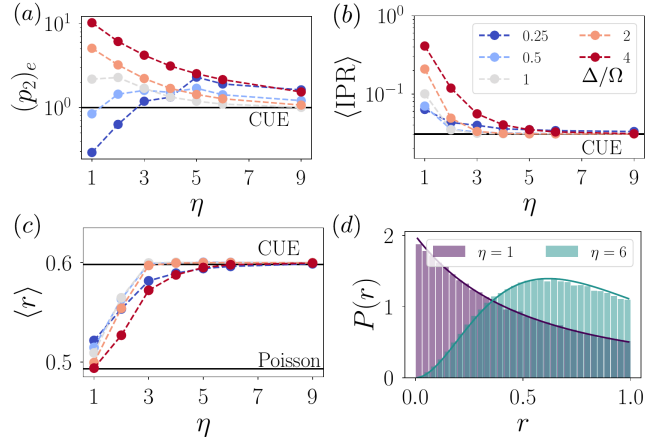


FIG. 9. *Comparison of different certification methods.* We use $N_U = 100$ random unitaries ($N_M = \infty$) created in a Quantum Ising model with $L = 6$ spins using random quenches with disorder strength Δ and the pure test state $|\psi_{AF}\rangle$, to investigate (a) the estimation purity, (b) the ensemble averaged IPR and (c) the mean value $\langle r \rangle$ of the phase spacing statistics $P(r)$, as a function of the depth η . In panel (d), we show $P(r)$ for two values $\eta = 1, 6$ of depth and disorder strength $\Delta/\Omega = 4$. Solid lines are theoretical curves for Poisson (purple) and CUE statistics (green) [37].

U_A , $\text{IPR}(|\phi_\nu\rangle \langle \phi_\nu|) = 1$ for $\nu = 1, \dots, N_A$, and minimal for a completely delocalized state $|\psi\rangle = 1/\sqrt{N_A} \sum_\nu |\phi_\nu\rangle$, $\text{IPR}(|\psi\rangle \langle \psi|) = 1/N_A$. In the following, we consider the ensemble averaged IPR, $\langle \text{IPR}(\rho_A) \rangle$. For unitary 2-designs, in particular thus for the CUE, one finds, using results of Ref. [56],

$$\langle \text{IPR}(\rho_A) \rangle_{\text{CUE}} = \frac{2}{N_A + 1} \left(\text{Tr} [\rho_A^2] + \sum_{\substack{\nu, \mu=1 \\ \text{with} \\ \nu > \mu}}^{N_A} (\rho_A)_\nu (\rho_A)_\mu \right). \quad (\text{G2})$$

where $(\rho_A)_\nu$ ($\nu = 1, \dots, N_A$) denote the eigenvalues of the density matrix ρ_A .

We now consider the phase spacing statistics of the eigenvalues of U_A . To avoid the non-trivial unfolding of the spectrum [42], we consider the related distribution $P(r)$ of consecutive phase gaps r [37] with

$$r = \frac{\min(\delta_\nu, \delta_{\nu+1})}{\max(\delta_\nu, \delta_{\nu+1})} \in [0, 1] \quad \text{with } \delta_\nu = \theta_{\nu+1} - \theta_\nu, \quad (\text{G3})$$

which provides information about the characteristic phase repulsion of chaotic quantum systems [42]. Here, the phase gaps δ_ν are obtained by first ordering the phases $\theta_\nu \in [-\pi, \pi]$ of the eigenvalues $e^{i\theta_\nu}$ and then calculating the difference between consecutive phases. Mean values of r for different random matrix ensembles are $\langle r \rangle_{\text{CUE}} \approx 0.53$ for the CUE and $\langle r \rangle_{\text{POI}} \approx 0.39$ for Poisson distributed phases [37].

In Fig. 9, we compare the different measures, using random unitaries created with random quenches in a Quan-

tum Ising model with $L = 6$ spins, short range interactions $\alpha = 6$ and various disorder strengths Δ . Quench time and interactions are fixed $JT = 1$, $J = \Omega$. We use a pure antiferromagnetic test state $|\psi_{AF}\rangle = |\uparrow\downarrow\dots\uparrow\downarrow\rangle$. In panels (a-c), we show the estimated purity, the IPR of $|\psi_{AF}\rangle$ and the average value of adjacent phase gaps, respectively, as a function of the number of quenches η . For a wide range of disorder strengths, we find convergence to the respective values expected for the CUE, indicating the convergence of the created ensemble of random unitaries towards the CUE. An optimal speed of convergence is obtained for $\Delta \approx J$ for all cases.

For a single quench $\eta = 1$, we observe that the dynamics described by $U_A = \exp(-iH_A^1 T)$ approached the MBL regime with increasing disorder $\Delta > J$: In panel (a), the estimation of the purity grows with Δ , indicating that the state is less randomized (delocalized) in the entire Hilbert space. This is confirmed in panel (b) by an IPR growing with Δ . Further, we find that $\langle r \rangle$ approaches with growing Δ the Poisson value, which represents a signature of many-body localization (see [37] and references therein). However, as shown in panel (d), we find that dynamics become chaotic with increasing number of quenches, even for strong disorder $\Delta/J = 4$. For $\eta = 1$ we obtain Poissonian statistics, whereas for $\eta = 6$ we observe phase repulsion described by Wigner's surmise [37].

In summary, we find that the estimation of the purity of known test states with our measurement protocol provides a method to test created ensembles of random unitaries, which is consistent with other theoretical tools like IPR and phase spacing statistics. Beyond the measurement of Rényi entropies, we emphasize that random quenches can be used as experimental tool to study the (fast) transition from localized to ergodic dynamics and many-body quantum chaos.

Appendix H: Scaling of statistical errors

In this section, we discuss statistical errors involved in global and local version of our protocol (see MT). In particular, we determine the necessary experimental resources, the number of measurements N_M per random unitary and number of random unitaries N_U , to estimate functionals $p_n = \text{Tr}[\rho_A^n]$ ($n \in \mathbb{N}$) of a density matrix ρ_A up to a given error threshold and the scaling of these numbers with system size.

1. Protocol using global random unitaries

To determine the statistical error involved in the global protocol, we assume that the reduced density matrix ρ_A of the subsystem A is defined in a Hilbertspace with dimension \mathcal{N}_A in which random unitaries $U_A \in \text{CUE}(\mathcal{N}_A)$ can be created. We consider further first random measurements of an observable \mathcal{O} with $N_{\mathcal{O}} = \mathcal{N}_A$ possible outcomes (i.e. $\text{Tr}[\mathcal{P}_{\mathbf{s}}^{\mathcal{O}}] = 1 \forall \mathbf{s}$ where $\mathcal{P}_{\mathbf{s}}^{\mathcal{O}}$ denote the

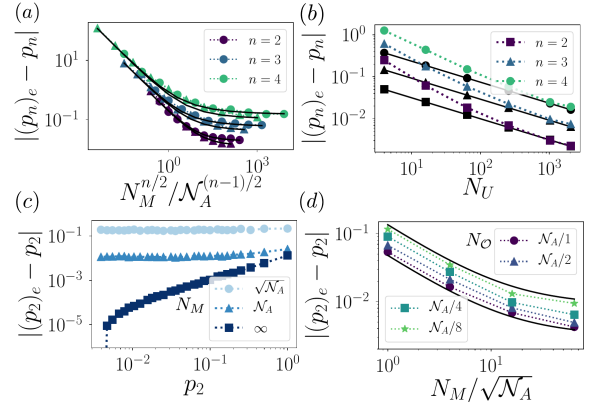


FIG. 10. *Scaling of statistical errors.* Average statistical error of an estimation of $p_n = \text{Tr}[\rho_A^n]$ as a function of a) the number of measurements N_M per unitary and b) the number of unitaries; in a) $N_U = 1000$, $\mathcal{N}_A = 64$ (dots) and $\mathcal{N}_A = 256$ (triangles), in b) $N_M = \infty$, $\mathcal{N}_A = 256$. c) Average statistical error of an estimation of $p_2 = \text{Tr}[\rho_A^2]$ as a function of the purity of the input state p_2 . Different colors correspond to different number of measurements N_M per unitary. $\mathcal{N}_A = 256$, $N_U = 100$. d) Average statistical error of an estimation of $p_2 = \text{Tr}[\rho_A^2]$ as a function of the number of measurements N_S per unitary for observables with different number of outcomes $N_{\mathcal{O}} = \mathcal{N}_A, \mathcal{N}_A/2, \mathcal{N}_A/4, \mathcal{N}_A/8$, with $\mathcal{N}_A = 256$, $N_U = 1000$. In all panels, unitaries were drawn directly from the CUE [57].

projector corresponding to a measurement outcome \mathbf{s}). We then extend to more general observables and discuss additionally the influence of the state ρ_A itself on the statistical error.

Finite number of measurements per unitary – Given a fixed random unitary U_A , we discuss first the faithful estimation of the probability $P \equiv \text{Tr}[U_A \rho_A U_A^\dagger \mathcal{P}_{\mathbf{s}}^{\mathcal{O}}]$ of an outcome \mathbf{s} and its powers P^n ($n \in \mathbb{N}$) using N_M measurements. In an experiment, P is obtained by performing N_M measurements on the state $U_A \rho_A U_A^\dagger$ and dividing the number of measurements, which have yield the outcome \mathbf{s} , by N_M . Mathematically, this is described by a random variable (an estimator) \tilde{P}

$$\tilde{P} \equiv \frac{1}{N_M} \sum_{i=1}^{N_M} \mathbf{1}_{\mathbf{s}}(\tilde{X}_i) \stackrel{d}{=} \frac{\tilde{B}(P, N_M)}{N_M} \quad (\text{H1})$$

Here, \tilde{X}_i is a random variable describing the i -th measurement and $\mathbf{1}_{\mathbf{s}}(\tilde{X}_i) = 1$ if $\tilde{X}_i = \mathbf{s}$ and $\mathbf{1}_{\mathbf{s}}(\tilde{X}_i) = 0$ if $\tilde{X}_i \neq \mathbf{s}$. $\tilde{B}(P, N_M)$ denotes a random variable distributed according to Binomial distribution with probability per trial P and number of trials N_M [58]. We note that the estimator \tilde{P} is faithful, $\mathbb{E}[\tilde{P}] = P$. In contrast, the simple power \tilde{P}^n is a biased estimator of P^n for $n > 1$, it overestimates for finite N_M , $\mathbb{E}[\tilde{P}^n] - P^n = \mathcal{O}(P/N_M^{n-1})$. A unique faithful estimator \tilde{P}_n is constructed using an ansatz $\tilde{P}_n = \sum_{k=0}^n \alpha_k \tilde{P}^k$ and the

defining condition $\mathbb{E} [\widetilde{P}_n] \stackrel{!}{=} P^n$. For example, one finds $\widetilde{P}_2 = \widetilde{P}(\widetilde{P}N_M - 1)/(N_M - 1)$ with $\mathbb{E} [\widetilde{P}_2] = P^2$. We use these unbiased estimators to simulate numerically an experiment with a finite number of measurements.

The average statistical error of an estimation of P^n using \widetilde{P}_n is given by its standard error $\sigma [\widetilde{P}_n]$. With the relation to the Binomial distribution, one finds for $1 \ll N_M \ll 1/P \approx \mathcal{N}_A$

$$\sigma [\widetilde{P}_n] = \sqrt{n!} \left(\frac{P}{N_M} \right)^{\frac{n}{2}} \left(1 + \mathcal{O} \left(\frac{1}{N_M}, PN_M \right) \right). \quad (\text{H2})$$

Finite number of unitaries – The estimation of $P_{U_{A,l}}^n \equiv \text{Tr} [U_{A,l} \rho_A U_{A,l}^\dagger \mathcal{P}_s^\mathcal{O}]^n$ ($l = 1, \dots, N_U$) is performed for N_U different random unitaries $U_{A,l}$. The resulting estimates $(P_{U_{A,l}}^n)_e$, each afflicted with an error of the order $\sigma [\widetilde{P}_n]$, are subsequently averaged to obtain $\langle P^n \rangle_e = 1/N_U \sum_{l=1}^{N_U} (P_{U_{A,l}}^n)_e$. This is an approximation of the average $\langle P^n \rangle$ of the exact probabilities over the entire CUE. Its average statistical error is in the limit $N_U \gg 1$ determined by the central limit theorem and given by

$$|\langle P^n \rangle_e - \langle P^n \rangle| \sim \frac{1}{\sqrt{N_U}} \left(\sigma [\tilde{P}_n] + C_n \right) \quad (\text{H3})$$

It consists of two parts. The former, $\sigma [\tilde{P}_n]$, has been already discussed and is caused by the finite number of measurements N_M per random unitary. The latter C_n originates solely from the finite number of random unitaries. As noted also in Ref. [21] for the case $n = 2$, it is state dependent, $C_n = C_n(\text{Tr} [\rho_A^n])$, largest for pure states and given by

$$C_n = \left(\langle P(s)^{2n} \rangle - \langle P(s)^n \rangle \right)^{1/2} \stackrel{\text{Tr}[\rho_A^n]=1}{=} \frac{n!}{\mathcal{N}_A^n} \left(\left[\binom{2n}{n} - 1 \right]^{\frac{1}{2}} + \mathcal{O} \left(\frac{1}{\mathcal{N}_A} \right) \right). \quad (\text{H4})$$

As a function of $\text{Tr} [\rho_A^n]$, C_n decreases polynomially. We discuss this and its influence on the total error of an estimation of $\text{Tr} [\rho_A^n]$ in detail below [see also Fig. 10, panel (d)].

Total error – Finally, an estimate $(p_n)_e$ is calculated using a (non-linear) function of all estimated $\langle P^k \rangle_e$ with $k \leq n$ (see App. A). Since, their statistical errors [equation (H3)] grow with k , we can estimate the scaling of total statistical error of $(p_n)_e$ from the error of the highest order polynomial $\langle P^n \rangle_e$. To account for the fact that the statistical errors of lower order polynomials are not independent, we introduce further adjustable prefactors. We find that the numerical data ($n = 2, 3, 4$) presented in Fig. 10, panels (a) and (b), and in Fig. (3) in the MT

is well described by

$$|(p_n)_e - p_n| \sim \frac{1}{\sqrt{N_U \mathcal{N}_A}} \left(C'_n + B_n \sum_{k=0}^{k < n/2} \left(\frac{\mathcal{N}_A}{N_M} \right)^{\frac{n}{2} - k} \right). \quad (\text{H5})$$

For $n = 2, 3, 4$, we find $C'_n \approx C_n/3(n-1)!$ and $B_n \approx \sqrt{n!}$ which increases exponentially with n . The additional global factor $1/\sqrt{\mathcal{N}_A}$ in the equation (H5), compared to (H3), originates from the fact that $(p_n)_e$ is calculated for each possible outcome s separately and an average over all $N_\mathcal{O} = \mathcal{N}_A$ outcomes has been taken.

To estimate p_n up to a fixed error ϵ , one needs hence to perform $N_M \sim \mathcal{N}_A^{\frac{n-1}{2}}$ measurements per unitary and average over $N_U \sim B_n^2/\epsilon^2$ unitaries. While the amount of necessary experimental resources increases thus exponentially with the order of the Rényi entropy n and system size, the measurement of low order Rényi entropies $n = 2, 3, 4$ in systems of moderate size is accessible, as exemplified by the various examples presented throughout the text.

Influence of the input state – We discuss now the influence of the input state on statistical errors. Hereby, we note that the random unitaries in the protocol are drawn from an ensemble which is invariant under unitary transformation (the CUE or an unitary n -design). By definition, average statistical errors of $(p_n)_e$ can hence only depend on properties of ρ_A which are invariant under unitary transformations, i.e. on the functionals p_n . Accordingly, we show in Fig. 10, panel (c), the average statistical error of the estimated purity $(p_2)_e$ as a function of the purity of the input state p_2 . In the case $N_M \rightarrow \infty$ (dark blue squares), the error due to the finite number of unitaries, which is proportional to C_2 , is dominating. It is decreasing polynomially with p_2 towards zero for a completely mixed state. However, in the experimentally most relevant scenario, $N_M \lesssim \mathcal{N}_A$, we find independence of the initial state.

Influence of the chosen observable – As estimates $(p_n)_e$ can be inferred from random measurements of any observable (see App. A), we finally discuss the influence of the chosen observable \mathcal{O} on the statistical error. We note that $(p_n)_e$ is calculated for each measurement outcome s separately [see equation (A3)]. Since in an experiment, the probabilities $P(s)$ are measured simultaneously for all possible measurement outcomes s , an average can be taken without further experimental effort. This reduces the error by a factor $1/\sqrt{N_\mathcal{O}}$ where $N_\mathcal{O}$ is the number of measurement outcomes. Hence, observables with the maximal number of outcomes $N_\mathcal{O} = \mathcal{N}_A$ are favorable. This is confirmed numerically, in Fig. 10, panel (d), where the error of the purity inferred from random measurements of observables with various numbers of possible outcomes are shown. Varying $N_\mathcal{O}$ lead for the statistical error of the purity to a simple rescaling $|(p_2)_e - p_2| \sim \left(C'_2 + B_2 \frac{\mathcal{N}_A}{N_M} \right) / \sqrt{N_U N_\mathcal{O}}$.

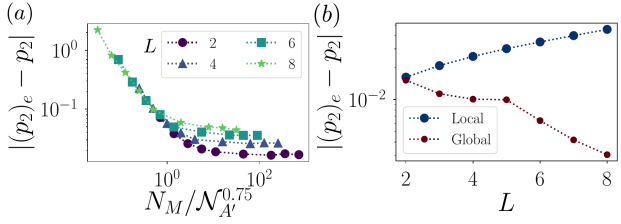


FIG. 11. *Scaling of statistical errors in the local protocol* We consider a partition of a spin-1/2-chain with L spins and total Hilbert space dimension $\mathcal{N}_A = 2^L$. (a) Error as a function of N_M , for various L , exhibiting the scaling $\mathcal{N}_A^{0.75}/N_M$ for $N_M \ll \mathcal{N}_A$. b) Comparison of the error in local and global protocol in the limit $N_M \rightarrow \infty$ as a function of the number of spins L . $N_U = 1000$ unitaries were drawn directly from the CUE [57].

2. Protocol using local random unitaries

We discuss now statistical errors involved in the estimation of the purity in the protocol based on unitaries $U_A = \bigotimes_i u_i$ with $u_i \in \text{CUE}(d_i)$ acting on a local constituent i of the subsystem A with local Hilbert space dimension d_i . As an example, we consider a spin-1/2-chain with L spins ($d_i = 2$) and total Hilbert space dimension $\mathcal{N}_A = 2^L$.

In Fig. 11 (a), we display the average statistical error of

the estimated purity of a reduced density matrix ρ_A as a function of the number of measurements N_M per random unitary, for various subsystem sizes and a fixed number of random unitaries $N_U = 1000$. In the limit $N_M \ll \mathcal{N}_A$ we find numerically a scaling of the statistical error of the estimated purity $\sqrt{N_U} |(p_2)_e - p_2| \sim \mathcal{N}_A^\kappa / N_M$ with $\kappa = 0.75 \pm 0.1$. Compared to the global protocol (scaling exponent $\kappa = 1/2$) the error is hence increased. In Fig. 11 (b), we further observe that in the limit $N_M \rightarrow \infty$, the error grows with increasing system size L , which is contrary to the global protocol (see also Fig. 3 MT). Both results are explained by the fact that in the local protocol the purity of the reduced density matrix ρ_A of a subsystem A is recursively determined from the purities of the reduced density matrices $\rho_{A'}$ of all subsystems $A' \subset A$ [see Eq. (5) MT]. Hence, their statistical errors add up. For larger systems, the number of involved subsystems increases, causing the growing statistical error.

To summarize, we find that the *local protocol*, compared to the global one, is more prone to statistical errors and requires thus more measurements per random unitary to obtain the purity of the reduced density matrix ρ_A of a subsystem A up to a given error. However, we obtain in addition the purities of all reduced density matrices $\rho_{A'}$ of subsystems $A' \subset A$ and hence more information than in the global version.